Atmos. Meas. Tech. Discuss., doi:10.5194/amt-2015-390, 2016
Manuscript under review for journal Atmos. Meas. Tech.
Published: 17 February 2016

Atmospheric Measurement Techniques Discussions

Real time retrieval of volcanic cloud particles and SO_2 by satellite using an improved simplified approach

S. Pugnaghi[1], L. Guerrieri[1], S. Corradini[2] and L. Merucci[2]

[1]{Dipartimento di Scienze Chimiche e Geologiche, Università di Modena e Reggio Emilia, 41125 Modena, Italy}

[2]{Istituto Nazionale di Geofisica e Vulcanologia, 00143 Roma, Italy}

Correspondence to: S. Pugnaghi (sergio.pugnaghi@unimore.it)

Abstract

Volcanic Plume Removal (VPR) is a procedure developed to retrieve the ash optical depth, effective radius and mass, and sulphur dioxide mass contained in a tropospheric volcanic cloud from the thermal radiance at 8.7, 11, and 12 μm. It is based on an estimation of a virtual image representing what the sensor would have seen in a multispectral thermal image if the volcanic cloud were not present. Ash and sulphur dioxide were retrieved by the first version of the VPR using a very simple atmospheric model that ignored the layer above the volcanic cloud. This new version takes into account the layer of atmosphere above the cloud as well as thermal radiance scattering along the line of sight of the sensor. In addition to improved results, the new version also offers easier and faster preliminary preparation and includes other types of volcanic particles. As in the previous version, a set of parameters regarding the volcanic area, particle types, and sensor are required to run the procedure. However, in the new version, only the mean plume temperature is required as input data. It this work a set of parameters have been computed for different types of plume particles (andesite, obsidian, pumice, ice, water, and sulphuric acid droplets), for both the Mt. Etna (Italy) and Eyjafjallajökull (Iceland) volcanoes, and for the MODIS Terra and Aqua instruments. Two different synthetic images, one for Mt. Etna and one for Eyjafjallajökull, are used to compare the results from the new and old procedures. Finally, a sensitivity analysis was conducted to investigate variations in VPR ash and sulphur dioxide retrievals as a function of plume altitude and particle type.

Atmos. Meas. Tech. Discuss., doi:10.5194/amt-2015-390, 2016
Manuscript under review for journal Atmos. Meas. Tech.
Published: 17 February 2016

Atmospheric Measurement Techniques Discussions

1. Introduction

The large volumes of ash mixed with various gases that can be released into the atmosphere during explosive volcanic eruptions sometimes form clouds that travel great distances from the source over long periods, carried by the wind. These ash clouds can be generated at any time from the eruption of any one of more than 1,200 active volcanoes scattered over the Earth's surface (Prata, 2009) and pose a real threat to air safety (Casadevall, 1994).

An effective global monitoring system today depends on the use of satellite data to detect and monitor the evolution of volcanic ash clouds. Timely information on the location, size, height, and ash content of potentially hazardous eruption clouds derived from satellite data are generated and used by the Volcanic Ash Advisory Centres (VAACs) to mitigate this type of threat and improve aviation safety (Francis et al., 2012).

Satellite sensors operating in the thermal infrared range are particularly effective for this purpose, when the interaction of volcanic ash with electromagnetic radiation makes it possible to detect and monitor volcanic clouds even at night. The algorithms developed exploit in various ways the reverse absorption of the brightness temperature observable in the channels centred at 10.8 and 12 microns. This feature is used both for discriminating ash and meteorological clouds (Prata 1989a, 1989b), and for quantifying the mass, optical thickness, and effective radius of the ash contained in volcanic clouds (Wen and Rose, 1994).

Several algorithms were developed in the early efforts to detect volcanic clouds and retrieve the ash and SO_2 contents, as discussed in a recent critical review (Clarisse and Prata, 2016). Among the new algorithms the simplified approach of the VPR is distinguished by its ease of use and speed of calculation, making it highly effective for monitoring. Another advantage of the VPR approach is that it only requires the plume temperature as additional input, providing fresh estimates of ash and SO_2 as soon as new satellite images of an ongoing eruption become available (Pugnaghi et al., 2013; Guerrieri et al., 2015).

The VPR procedure was developed using thermal infrared (TIR) data collected by the Moderate Resolution Imaging Spectroradiometer (MODIS) instrument on board the Terra and Aqua polar platforms, and by the Spinning Enhanced Visible and Infra Red Imager radiometer (SEVIRI) on board meteorological satellites positioned on MSG geostationary orbits.

This paper aims to present the VPR procedure in an improved and simplified form as developed for the selected case studies of the Mt. Etna (Italy) and Eyjafjallajökull (Iceland) eruptions. Section 2 is dedicated to a theoretical description of the novel improvements of the VPR procedure, while section 3 presents and discusses the results obtained for the validation case studies. Section 4 provides

Atmos. Meas. Tech. Discuss., doi:10.5194/amt-2015-390, 2016
Manuscript under review for journal Atmos. Meas. Tech.
Published: 17 February 2016

conclusions. Further theoretical details are included in Appendix A, while the VPR coefficients are tabulated in Supplement for different types of plume particles (andesite, obsidian, pumice, ice, water, and sulphuric acid droplets), for both the Mt. Etna and Eyjafjallajökull volcanoes, and for the MODIS Terra and Aqua instruments.

2. Theory

The Volcanic Plume Removal (VPR) procedure (Pugnaghi et al. 2013; Guerrieri et al. 2015) is a linearization of the radiative transfer equation developed to retrieve, from multispectral satellite images at 8.7, 11, and 12 μm, the ash optical depth at 550 nm (δ^*), effective radius (R_e), mass (M_a), and sulphur dioxide mass (M_s) of a tropospheric volcanic cloud. The parameters required to apply the VPR are specific for a given volcano, type of plume particles, and sensor on board the satellite and these are easily determined *a priori* using the MODTRAN radiative transfer model. Once they have been computed, the only additional inputs required are the multispectral image and the mean plume temperature.

Figure 1 shows the VPR procedure flowchart (dashed rectangle). The land-sea mask is usually available with the radiance data while the operator has to define the plume mask and possibly the meteorological cloud mask. For the multispectral sensors the plume mask can be derived from ash detection techniques based on Brightness Temperature Difference (BTD, see Prata, 1989b) and successive improvements (see Millington et al., 2012, Pavolonis et al., 2013), principle components analysis (Hillger and Clark 2002a,b), or neural networks (Picchiani et al., 2014). The volcanic cloud temperature input data can be obtained from VIS/TIR ground-based cameras (Scollo et al., 2014), ground radar (Montopoli et al., 2014; Marzano et al., 2006; Corradini et al., 2015), lidar system (Scollo et al., 2012) measurements, or from multispectral satellite data using different techniques like *dark pixels* (Prata and Grant, 2001; Corradini et al., 2010), CO_2 slicing (Menzel et al., 1983; Platnick et al., 2003), H_2O intercept method (Nieman et al., 1993), tracking of volcanic cloud centre of mass (Guerrieri et al., 2015), or inversion schemes based on Optimal Estimation (Francis et al., 2012).

The first step of the VPR is definition of the virtual image with the removed volcanic cloud and computation of plume transmittances for the three bands considered (8.7, 11, and 12 μm). In the earlier VPR approach, the atmosphere above the plume was assumed to be negligible and the results were adjusted with a cubic relationship, derived by fitting an adequate set of MODTRAN simulations (Pugnaghi et al. 2013; Guerrieri et al. 2015). The transmittance values at 11 and 12 μm were used to define maps of R_e, δ^* and M_a, while the sulphur dioxide abundance map was estimated from the

Atmos. Meas. Tech. Discuss., doi:10.5194/amt-2015-390, 2016
Manuscript under review for journal Atmos. Meas. Tech.
Published: 17 February 2016

Atmospheric Measurement Techniques
Discussions

transmittance at 8.7 μm. Finally, the wind speed at the plume altitude was used to reconstruct the flux at the vents, considering both the ash mass and SO_2 maps (Merucci et al., 2013; Guerrieri et al., 2015; Merucci, 2015).

The novel VPR procedure described here applies a new atmospheric model for estimating volcanic cloud transmittance (white box, inside the dashed square in Fig. 1). Here both the transmittance τ'' and the up-welling radiance L''_{uo} of the layer of atmosphere above the plume are considered (as shown in the scheme in Fig. 2). The term representing the surface thermal radiance scattered by the volcanic particles along the line of sight of the sensor is now also considered (not shown in the scheme of Fig. 2).

With this atmospheric model, the plume radiance $\boldsymbol{L_p}$ measured by the sensor can be approximated by the parabolic trend (see Appendix A for a detailed description):

$$L_p = -\alpha \cdot \tau_p^2 + \left[L_o + \alpha - B_p \cdot \tau'' - L''_{uo}\right] \cdot \tau_p + \left[B_p \cdot \tau'' + L''_{uo}\right] \qquad (1)$$

where α is a term mainly proportional to $\varepsilon \cdot B(T_s) \cdot \tau$; ε is the surface emissivity, $B(T_s)$ is the Planck emission at the surface temperature T_s, and $\tau = \tau' \cdot \tau''$ is the transmittance of the whole atmosphere (α also depends on the aerosol optical depth, but this effect is important mainly for very optically thick pixels); L_o is the radiance at the sensor with the plume removed; B_p is the Planck emission at the mean plume temperature T_p; $\tau_p = \tau_a \cdot \tau_s$, is the plume transmittance where τ_a is the aerosol transmittance, and τ_s is the part due to sulphur dioxide. From these definitions it follows that if SO_2 is absent then $\tau_s = 1$; and if the aerosol optical depth $\delta = 0$, then $\tau_a = 1$.

2.1 Absence of sulphur dioxide

If sulphur dioxide is absent or if only the thermal bands not affected by SO_2 are considered, in Eq. (1) τ_p can be substituted with τ_a representing only the ash component.

Fig. 3a shows a series of MODTRAN simulated radiances at the sensor versus the plume transmittance obtained specifically for the band at 11 μm of the MODIS-Aqua sensor, pumice (Volz, 1973) ash type, and a set of possible plume configurations (see Supplement for details).

The parameter values of the parabolic fit of the radiance L_p versus the plume transmittance τ_a shown in Fig. 3a, $L_p \cong \sum_{i=0}^{2} a_i\,(\tau_a)^i$, are reported in Table 1. By definition: $a_0 + a_1 + a_2 = L_0$. In this case the sum is 8.57 (W m^{-2} sr^{-1} μm^{-1}), as can be seen in Fig. 3 for $\tau_a = 1$.

Atmos. Meas. Tech. Discuss., doi:10.5194/amt-2015-390, 2016
Manuscript under review for journal Atmos. Meas. Tech.
Published: 17 February 2016

The parabolic trend shown in Fig. 3a changes according to the state of the atmosphere, the surface characteristics and, of course, the position of the volcanic cloud, composition, and ash content. Approximating the radiance L_p expressed as a function of the plume transmittance τ_a with two linear trends, for high radiance values (i.e. the transparent pixels of the plume) and for low values (more opaque plume pixels), if the surface characteristics do not vary excessively over time, it can be observed that the linear trends always intersect close to the same transmittance value (named τ_t). Figure 3b shows that $\tau_t \approx 0.3$. Clearly, the gains and offsets of these two linear trends also change according to the state of the atmosphere, plume temperature, and so on. These two linear fits, are characterised by four parameters. However, only the offset (named B_{up}) is required to fit the transparent part because the radiance L_0 is known from the plume removal part of the procedure. Similarly, if the intersection point of the two linear trends is known, the offset of the opaque part (named B_{dn}) is sufficient to determine the linear fit.

Summarising, by knowing the air temperature T_p at the mean plume altitude (thus B_p term) and the radiance $L_o$with the plume removed, it is possible to estimate the aerosol plume transmittance τ_a directly from the radiance measured by the satellite (without atmospheric correction or radiative transfer models) using Eq. (2) (red line) and, if necessary, Eq. 3 (blue line) of Fig. 3b:

$$L_p = \left[L_o - B_{up}\right] \cdot \tau_a + B_{up} \quad (2)$$

If the computed transmittance τ_a is lower than τ_t (intersection point), then the plume transmittance is recomputed by:

$$L_p = [(L_t - B_{dn})/\tau_t] \cdot \tau_a + B_{dn} \quad (3)$$

where L_t is the radiance at the sensor computed using Eq. (2) for a plume transmittance $\tau_a = \tau_t$. Figure 4a shows that in the 11 µm band there is a linear relationships between the two aforementioned offsets B_{up} , B_{dn} and the Planck emission of the plume B_p. A similar relationship also exists for the other two bands (obviously, for the band centred at 8.7 µm, sulphur dioxide must be absent) and for other volcanic particle types (see Supplement). Figure 4a also shows that the plume transmittance at the intersection point τ_t is almost constant with only a small dependence on B_p.
Therefore:

$$B_{up} = a_{up} \cdot B_p + b_{up} \quad (4)$$

$$\tau_t = a_{tt} \cdot B_p + b_{tt} \quad (5)$$

$$B_{dn} = a_{dn} \cdot B_p + b_{dn} \quad (6)$$

2.2 Presence of sulphur dioxide

The presence of sulphur dioxide complicates transmittance retrieval at 8.7 µm because weak SO_2 absorption affects this band. If the aerosol component of the plume transmittance at 8.7 µm is known, then the radiance at the sensor without the presence of sulphur dioxide L_a can be computed using the Eqs. (2) and (3). A knowledge of radiance due only to aerosols makes it possible to define the following simple equation:

$$L_p = [L_a - B_s] \cdot \tau_s + B_s \quad (7)$$

where L_p is the total plume radiance measured by the sensor, L_a is radiance due to the aerosol components of the plume, and τ_s is the plume transmittance due to SO_2 absorption. B_s is a constant which takes into account the plume temperature, plume position, and state of the atmosphere above the plume and it is computed using a linear function of B_p:

$$B_s = a_s \cdot B_p + b_s \quad (8)$$

Figure 4b shows the trend of B_s versus B_p derived from a complete dataset of MODTRAN simulations for Mt. Etna measured with a MODIS-Aqua instrument.

Therefore, to compute τ_s from Eq. (7), it is necessary to know L_a which is derived from Eqs. (2) and (3) when τ_a for the band at 8.7 µm is known. The transmittance τ_a can easily be computed for pumice-type ash particles because a very good correlation exists between $\tau_{a,8.7}$ and $\tau_{a,11}$ (see Fig. 5a, and Pugnaghi et al. 2013). The fit is a cubic polynomial: $\tau_{a,8.7} = \sum_{i=0}^{3} a_{i,8.7} \left(\tau_{a,11}\right)^i$ and the parameter values from the MODIS sensors on board the Terra and Aqua satellites are reported in Table 2. These parameters are an improved version of those reported in Pugnaghi et al. (2013), because in the first version of the VPR the thermal radiance scattered along the line of sight of the sensor was ignored.

Atmos. Meas. Tech. Discuss., doi:10.5194/amt-2015-390, 2016
Manuscript under review for journal Atmos. Meas. Tech.
Published: 17 February 2016

Atmospheric Measurement Techniques Discussions

Unfortunately, for other particle types (see Supplement), the correlation between $\tau_{a,8.7}$ and $\tau_{a,11}$ is not always good, as in the example of Fig. 5b showing the scatter plot for water droplets. Nevertheless, it should be noted that this correlation becomes very good if only particles of the same effective radius R_e are considered.

In these cases with non-pumice ash types, the aerosol transmittance $\tau_{a,8.7}$ at 8.7 μm can be obtained from the formula:

$$\tau_{a,8.7} = e^{-\mu \cdot \delta_{8.7}} = e^{-\mu \cdot m_{8.7} \cdot \delta^*} \tag{9}$$

where μ is the optical air mass factor, $\delta_{8.7}$ is the vertical optical depth, δ^* is the vertical optical depth at 550 nm, and $m_{8.7}$ is the gain of the linear relationship which gives the optical depth $\delta_{8.7}$, when δ^* is known; the gain $m_{8.7}$ is a function of the effective radius R_e and is known from the MODTRAN simulations (Guerrieri et al., 2015).

To sum up, the novel VPR procedure first computes the 11 and 12 μm band transmittances (as indicated in the flowchart of Fig. 1), and from these the aerosol optical depth at 550 nm (δ^*) and the effective radius (R_e) of each pixel of the plume (Pugnaghi et al. 2013); then the aerosol transmittance at 8.7 μm ($\tau_{a,8.7}$) is obtained using Eq. (9).

Finally, the transmittance $\tau_{s,8.7}$ (derived from Eq. 7) is used to estimate the SO_2 columnar abundance C_s, given the proper absorption coefficient β (Pugnaghi et al. 2013) and the optical air mass μ factor.

$$\tau_{s,8.7} = e^{-\mu \cdot \beta \cdot C_s} \tag{10}$$

The subsequent steps of the VPR procedure have not been changed and can be found in Pugnaghi et al., (2013). Nevertheless, to conclude the theoretical discussion, it is important to note the superposition effect of ash and sulphur dioxide on the radiance measured by the sensor. This means that the proposed VPR procedure can also work well in cases of a *double-plume* at different temperatures, for example if an ash plume is located directly above or below a sulphur dioxide plume.

3. Validation test cases

To test the improved version of the VPR procedure two trial synthetic images were defined as described in Corradini et al. (2014), for both the MODIS-Aqua effective wavelengths, depicting a uniform ocean surface under a cloudless sky, and a plume of known spherical particles.

Atmos. Meas. Tech. Discuss., doi:10.5194/amt-2015-390, 2016
Manuscript under review for journal Atmos. Meas. Tech.
Published: 17 February 2016

The first image is characterized by an atmospheric situation, ocean temperature, and the particle type typical of the Sicilian Mt. Etna volcano, while the second is adapted to match the Icelandic Eyjafjallajökull volcano. Figure 6 shows the two RGB colour composite synthetic images with the radiances of the channels centred at 8.7, 11, and 12 μm respectively. The left plate shows the Mt. Etna scenario with a plume of the same shape as the volcanic cloud detected by MODIS-Aqua during the 26 October 2013 eruption at 12:20 GMT. The right plate shows the Eyjafjallajökull scenario, depicting a portion of the Eyjafjallajökull plume detected by MODIS-Aqua on 11 May 2010 at 14:05 GMT.

3.1 The Mt Etna-Pumice scenario

The synthetic atmosphere in the Mt. Etna image in Fig. 6a is derived from the radiosonde pressure, temperature, and humidity (PTH) profiles measured by the Trapani (western tip of Sicily, Italy) WMO station 16429 on 26 October 2013 at 12 GMT, while the plume mask and the vertical zenith angles used to prepare the synthetic image are derived from the actual MODIS-Aqua data collected on October, 26, 2013 at 12:20 GMT. The plume in the synthetic image is defined as 1 km thick, located between 7 and 8 km, containing pumice ash (Volz, 1973) and SO_2. It has a Gaussian shape moving from the centre to the edge and ranging from 10 to 1 g m^{-2} columnar SO_2 abundance, and from 1.5 to 0.1 ash optical depth $\boldsymbol{\delta}^*$ (AOD at 550 nm). Therefore, a minimal quantity of sulphur dioxide and ash is always present in the plume, and the effective radii R_e of the particles have a uniform distribution, on a logarithmic scale, in the range 0.8-7 μm.

Table 3 shows that by excluding the SO_2 total mass, all the retrieval values of the new version of the VPR are closer to the true values than the old version. Both versions estimate a lower mass of ash in the volcanic cloud, but this probably also implies a greater burden of SO_2 detected with the old VPR. The retrieval of the total ash mass computed with the new VPR is better not only because it is closer to the true value, but also because both the estimated effective radius and optical depth used in mass estimation are closer to the true values.

Figure 7 shows the scatter plots of R_e, δ^*, M_a, and M_s versus the true values (synthetic image). All the scatter plots show a widening dispersion with increasing values. Fig. 8 reports (on the left) the trends of R_e and δ^* mean values retrieved with VPR using different input plume altitudes, and on the right the trends of ash and SO_2 total mass. As described in Pugnaghi et al. (2013), Guerrieri et al. (2015), and Merucci (2015), the effective radius and aerosol optical depth at 550 nm are derived from the transmittances retrieved at 11 and 12 μm, and then the ash mass is computed in each pixel with the Wen and Rose (1994) simplified formula. The trend of R_e versus volcanic cloud altitude is almost flat, while the optical depth δ^* shows a clear drop with height. The best retrieval (closest to true values) is at 7 km rather than the height used of 7.5 km. This is also true for SO_2 total mass.

Figure 9 shows the VPR retrievals for the Mt. Etna scenario giving as input the right plume temperature and all the types of particles reported in Tables S1, S2, S3, S5, S6, S7 (see Supplement). The upper plates show the mean effective radius (R_e, left) and the mean optical depth (δ^*, right). The lower plates show the retrievals of ash (left) and SO_2 (right) total mass. Among the different types of ash, andesite gives the worst effective radius and optical depth results, with respect to the true values. Nevertheless, because the two retrieved variables R_e and δ^* compensate each other, all the ash types considered give good estimations of the ash total mass. Conversely, for ice and water the results retrieved for the total mass are much higher and divergent from true values. Finally, by varying the ash type, the total ash mass exhibits a much lower variability when compared to that of SO_2.

3.2 The Eyjafjallajökull-Andesite scenario

The second synthetic image shown in Fig. 6b was created considering the state of the atmosphere derived from the PTH vertical profiles measured at Keflavik (WMO station 04018) on 11 May 2010 at 12:00 GMT. On that day, MODIS-Aqua captured the Eyjafjallajökull eruption during its transit at 14:05 GMT. As in the previous Mt. Etna eruption, the plume mask and the vertical zenith angles used in the synthetic image derive from the actual MODIS-Aqua data. The plume was again 1 km thick, but located lower than the previous case at between 4 and 5 km, containing spherical particles of andesite (Pollack et al. 1973) and SO_2. The same ranges and distributions of SO_2 columnar content, ash optical depth δ^* at 550 nm, and effective radius R_e were used, as for Mt. Etna.

Once again Table 4 demonstrates that the new version of the VPR generates better estimations compared to the old one, with all the parameters exhibiting difference percentages lower than 10%. The older version detects the presence of ash in a smaller number of pixels, but its greater effective radius and optical depth partly compensate for the smaller number of detected ash plume pixels in the final mass estimation.

The numbers of detected pixels for the sulphur dioxide component are in close agreement with the true value in both versions, and they retrieve a similar total mass of SO_2.

Figure 10 shows the scatter plots of R_e, δ^*, M_a, and M_s versus the true values. The correlation is quite good up to about $R_e = 5$ µm, $\delta^* = 1$, $M_a = 10\ gm^{-2}$, and $M_s = 7\ gm^{-2}$; wider dispersions can be observed for higher values.

Atmos. Meas. Tech. Discuss., doi:10.5194/amt-2015-390, 2016
Manuscript under review for journal Atmos. Meas. Tech.
Published: 17 February 2016

Atmospheric Measurement Techniques Discussions

Fig. 11 shows the trends of the VPR R_e and δ^* mean values (left), and total M_a and M_s (right) retrieved as functions of the input plume altitude. R_e and δ^* retrievals exhibit opposite trends which compensates each other, making the final retrieval of total ash mass less sensitive to plume altitude. In fact, from 3 to 5 km the ash mass ranges between 11 and 15 kt with a true value of about 13 kt. Only the optical depth at the right plume altitude (4.5 km) is very close to the true value. The best effective radius is at a mean plume altitude greater than 5 km and the best total mass is at about 4 km. However, the result obtained appears to be the best compromise. A greater plume height (e.g. 5 km) would mean a better R_e but a worse δ^* and also a worse total mass. Conversely, a lower plume height (e.g. 4 km) yields to very good total mass, but worse R_e and δ^* values.

Finally, as for Mt. Etna, the VPR results were considered using as input the actual plume temperature and all the types of particles reported in Supplement, including the Eyjafjallajökull ash type (Peters, 2013, referred in the figures as Eyja ash). In Fig. 12 the upper plates show the mean effective radius R_e (left) and optical depth δ^* (right) versus the different types of particles; the lower plates show the retrievals of ash and SO_2 total mass.

Only andesite and Eyjafjallajökull ash types give good results in both mean effective radius and optical depth, while obsidian is reasonably good only for the first parameter. The ash total mass exhibits quite constant values between 10 to 15 kt for all the four ash types, close to the true value of 13 kt. Vice versa, the total mass values retrieved for ice and water droplets were much higher and very different from the true values. As noted in the previous Etna scenario, their reciprocal difference is mainly due to different radius thresholds used in the procedure for water droplets and ice. The performance of sulphur dioxide total mass retrieval is seen to be strongly affected by the type of particle used in the procedure. Only andesite gives a good result in this case. Finally, sulphuric acid retrieval performance is different from both ash and the water-ice pair.

4. Conclusions

The new version of the VPR presented here is an approximated procedure. It uses only the mean altitude cloud temperature as input to directly interpret MODIS-TIR multispectral images and retrieve particle effective radius, optical depth, mass of the particle utilized, and mass of sulphur dioxide contained in each pixel of the volcanic cloud. The VPR approach requires no atmospheric correction because this is implicit in the procedure itself. The retrieval of effective radius, optical depth, and sulphur dioxide abundance is derived from estimation of plume transmittances in the bands centred at 8.7, 11, and 12 μm. This article presented a novel and effective improvement in the transmittance

Atmos. Meas. Tech. Discuss., doi:10.5194/amt-2015-390, 2016
Manuscript under review for journal Atmos. Meas. Tech.
Published: 17 February 2016

Atmospheric Measurement Techniques
Discussions

estimation scheme. In the new VPR, plume transmittance is obtained from the radiance measured by the sensor using two simple linear relationships; one for the most transparent part of the plume and one for the most opaque. These two linear trends account for two minor terms not considered in the previous version: the layer of atmosphere above the plume and the thermal radiance scattered along the line of sight of the sensor. Approximation for very thick/opaque volcanic clouds (transmittances lower than 0.05) is less effective. The improvement only involves the computation of volcanic cloud transmittance, and no other parts of the previous procedure have been modified. Nevertheless, the improvement has a dual positive effect: 1) it is simpler to use and provides more accurate results than before; 2) the preliminary work to compute the parameters required by the procedure (the parameters reported in Supplement) is easier than before and requires less processing time. The new VPR procedure was assessed against the older version by applying it to synthetic images generated using two real examples from the Mt. Etna (Italy) and Eyjafjallajökull (Iceland) volcanoes. The percentage difference between the average input data of the synthetic images and the mean results of the improved VPR ranges between 2-13 % for both Mt. Etna and Eyjafjallajökull, while the old VPR produced ranges between 4-68 % (see Tables 3 and 4), confirming the improved performance of the new version.

The correlation coefficient between the transmittance of the volcanic cloud simulated by MODTRAN and the corresponding transmittance retrieved by VPR is reported in the last column of tables S1 to S7, in nearly all cases this being close to one. However, the mean percentage errors of the retrieved effective radius, optical depth, ash mass, and sulphur dioxide mass expected in a real example may be greater than those reported in Tables 3 and 4. This is because the two synthetic images considered here exhibit a uniform and perfectly clear sky, a uniform ocean surface, and a volcanic cloud comprised of known spherical ash particles.

Appendix A

The radiance at the sensor when the volcanic cloud is absent is (see Fig. 2):

$$L_o = [\varepsilon\, B(T_s) + (1-\varepsilon)\, L_d] \cdot \tau + L_{uo} \qquad \text{(A1)}$$

Atmos. Meas. Tech. Discuss., doi:10.5194/amt-2015-390, 2016
Manuscript under review for journal Atmos. Meas. Tech.
Published: 17 February 2016

Atmospheric Measurement Techniques Discussions

where: ε is the surface emissivity; $B(T_s)$ is the Planck function at the surface temperature T_s; L_d is the atmospheric down-welling radiance; τ is the total atmospheric transmittance; L_{uo} is the total atmospheric up-welling radiance.

$$\tau = \tau' \cdot \tau'' \qquad \text{(A2)}$$

$$L_{uo} = L'_{uo} \cdot \tau'' + L''_{uo} \qquad \text{(A3)}$$

The radiance at the sensor when the volcanic cloud is present is:

$$L_p = [\varepsilon\, B(T_s) + (1-\varepsilon)\, L_d] \cdot \tau \cdot \tau_p + L_u + S \qquad \text{(A4)}$$

where: τ_p is the volcanic cloud transmittance; L_u is the current atmospheric up-welling radiance; S is the term accounting for the scattering of thermal radiance along the line of sight of the sensor.

Since surface emissivity is close to 1 (particularly above the ocean), the change of L_d in the presence of a volcanic cloud was ignored.

The atmospheric up-welling radiance in the presence of a volcanic cloud is:

$$L_u = L'_{uo} \cdot \tau_p \cdot \tau'' + L_{up} \cdot \tau'' + L''_{uo} \qquad \text{(A5)}$$

and, assuming $L_{up} = B_p \cdot (1 - \tau_p)$ where B_p is the Planck function at temperature T_p (air temperature at the mean plume altitude):

$$L_u = \{L_{uo} - [B_p \cdot \tau'' + L''_{uo}]\} \cdot \tau_p + [B_p \cdot \tau'' + L''_{uo}] \qquad \text{(A6)}$$

Indicating with P a degree of probability of the thermal radiation being scattered along the line of sight of the sensor, the scattering term was modelled as:

$$S = \left\{ \int_{\tau_p}^{1} [\varepsilon\, B(T_s) \cdot \tau' \cdot \tau_p] \cdot P\, d\tau_p' \right\} \cdot \tau'' = \alpha \cdot \tau_p \left(1 - \tau_p\right) \quad \text{(A7)}$$

where: $\alpha = \varepsilon\, B(T_s) \cdot \tau \cdot P$.

Here P is assumed to be constant even if it is a function of the ash/particle characteristics and therefore of τ_p itself. Clearly $P = 0$ if $\tau_p = 1$.

Inserting Eqs. (A6) and (A7) in (A4):

$$L_p = [\varepsilon\, B(T_s) + (1-\varepsilon)\, L_d] \cdot \tau \cdot \tau_p + \{L_{uo} - [B_p\, \tau'' + L''_{uo}]\} \cdot \tau_p + [B_p\, \tau'' + L''_{uo}] + \alpha \cdot \tau_p \left(1 - \tau_p\right) \quad \text{(A8)}$$

Finally, recalling Eq. (A1), Eq. (1) is obtained.

Acknowledgements

This work was partially funded by the European Union's Seventh Framework Programme (FP7/2007-2013) through the project APho-RISM (Advanced PRocedures for volcanIc and Seismic Monitoring) under grant agreement number 606738.

The authors would like to thank Gavin Taylor for carefully reading the original manuscript and for providing language corrections.

References

Casadevall, T. J.: The 1989–1990 eruption of Redoubt Volcano, Alaska: impacts on aircraft operations, J. Volcanol. Geotherm. Res., 62, 301–316, 1994.

Clarisse, L., and Prata, A. J.: Infrared sounding of volcanic ash. In: Mackie, Ricketts, Watson, Cashman and Rust (Eds.), Volcanic Ash: Hazard Observation. Elsevier, Oxford, 2016 (in press).

Corradini, S., Merucci, L., Prata, A. J., and Piscini, A.: Volcanic ash and SO2 in the 2008 Kasatochi eruption: retrievals comparison from different IR satellite sensors, J. Geophys. Res., 115, D00L21, 2010.

Corradini, S., Pugnaghi, S., Piscini, A., Guerrieri, L., Merucci, L., Picchiani, M., Chini M.: Volcanic Ash and SO2 retrievals using synthetic MODIS TIR data: comparison between inversion procedures and sensitivity analysis, Annals of Geophysics, Special Issue on "Atmospheric Emissions from Volcanoes", Vol. 57, Fast Track 2, doi: 10.4401/ag-6616, 2014.

Corradini, S., Montopoli, M., Guerrieri, L., Ricci, M., Scollo, S., Merucci, L., Marzano, F. S., Pugnaghi, S., Prestifilippo, M., Ventress, L., Grainger, R. G., Carboni, E., Vulpiani, G., Coltelli, M.: A multi-sensor approach for the volcanic ash cloud retrievals and eruption characterization, submitted to Remote Sensing, Special Issue on Volcano Remote Sensing, September 2015.

Durant, A. J., Shaw, R. A., Rose, W. I., Mi Y., and Ernst, G. G. J.: Ice nucleation and overseeding of ice in volcanic clouds, J. Geophys. Res.,113, D09206, doi:10.1029/2007JD009064, 2008.

Francis, P. N., Cooke, M. C. and Saunders, R. W.: Retrieval of physical properties of volcanic ash using Meteosat: A case study from the 2010 Eyjafjallajökull eruption, J. Geophys. Res., 117, D00U09, doi:10.1029/2011JD016788, 2012.

Guerrieri, L., Merucci, L., Corradini, S., and Pugnaghi, S.: Evolution of the 2011 Mt. Etna ash and SO2 lava fountain episodes using SEVIRI data and VPR retrieval approach, Journal of Volcanology and Geothermal Research, Vol. 291, pp. 63-71, doi:10.1016/j.jvolgeores.2014.12.016, 2015.

Hillger, D. W. and Clark, J. D.: Principal component image analysis of MODIS for volcanic ash. Part I: Most important bands and implications for future GOES Imagers, J. Appl. Meteorol., 41(10), doi: 10.1175/1520-0450(2002)041h0985:PCIAOMi2.0.CO;2, 2002a.

Hillger, D. W. and Clark, J. D.: Principal component image analysis of MODIS for volcanic ash. Part II: Simulation of current GOES and GOES-M imagers, J. Appl. Meteorol., 41(10), doi: 10.1175/1520-0450(2002)041h1003:PCIAOMi2.0.CO;2, 2002b.

Marzano, F. S., Barbieri, S., Vulpiani, G., and Rose, W. I.: Volcanic ash cloud retrieval by ground-based microwave weather radar, IEEE Trans. Geosci. Remote Sens., 44, 3235–3246, doi: 10.1109/TGRS.2006.879116, 2006.

Menzel, W. P., Smith, W. L., and Stewart, T. R.: Improved cloud motion wind vector and altitude assignment using VAS, Journal of Applied Meteorology, 22, 377-384, 1983.

Merucci, L., Volcanic risk mitigation and insights into volcanic processes from space-based measurements, PhD. Thesis, Università degli Studi di Modena e Reggio Emilia, ESS XXVII ciclo, 2015.

Merucci, L., Burton, M., Corradini, S., and Salerno, G.G.: Reconstruction of SO2 flux emission chronology from space-based measurements, Journal of Volcanology and Geothermal Research 206 (3-4): 80–87. doi:16/j.jvolgeores.2011.07.002, 2011.

Millington, S. C., Saunders, P. N. F. R. W., and Webster H. N.: Simulated volcanic ash imagery: A method to compare NAME ash concentration forecasts with SEVIRI imagery for the Eyjafjallajokull eruption in 2010, J. Geophys. Res., 117:D00U17, doi: 10.1029/2011JD016770, 2012.

Montopoli, M., Vulpiani, G., Cimini D., Picciotti, E., and Marzano, F. S.: Interpretation of observed microwave signatures from ground dual polarization radar and space multi-frequency radiometer for the 2011 Grímsvötn volcanic eruption, Atmos. Meas. Tech. 7, 537–552, doi:10.5194/amt-7-537-2014, 2014.

Nieman, S. J., Schmetz, J. and Menzel, W. P.: A comparison of several techniques to assign heights to cloud tracers. J. Appl. Meteor., 32, 1559-1568, 1993.

Pavolonis, M., Heidinger, A., and Siegla_ J.: Automated retrievals of volcanic ash and dust cloud properties from upwelling infrared measurements, J. Geophys. Res., 118(3):1436-1458, doi: 10.1002/jgrd.50173, 2013.

Peters, D., EODG-AOPP, University of Oxford, Private communication, 2013.

Picchiani, M., Chini, M., Corradini, S., Merucci, L., Piscini, A. and Del Frate, F.: Neural network multispectral satellite images classification of volcanic ash plumes in a cloudy scenario, Annals of

Geophysics, Special Issue on "Atmospheric Emissions from Volcanoes", Vol. 57, Fast Track 2, doi: 10.4401/ag-6638, 2014.

Platnick, S., King, M. D., Ackerman, S. A., Menzel, W. P., Baum, B. A., Riédi, J. C., and Frey, R. A.: The MODIS Cloud Products: Algorithms and Examples from Terra. IEEE Transactions on Geoscience and Remote Sensing, 41, 459-473, 2003.

Pollack, J., Toon, O., and Khare, B.: Optical properties of some terrestrial rocks and glasses. Icarus, 19, 372-389, doi: 10.1016/0019-1035(73)90115-2, 1973.

Prata, A. J.: Observations of volcanic ash clouds in the 10-12 μm window using AVHRR/2 data, Int. J. Remote Sens., 10, 751–761, 1989a.

Prata, A. J.: Infrared Radiative Transfer Calculations for Volcanic Ash Clouds, Geophys. Res. Lett., 16, 1293–1296, 1989b.

Prata, A. J., and Grant, I. F.: Determination of mass loadings and plume heights of volcanic ash clouds from satellite data, CSIRO Atmospheric Research Technical Papers No. no. 48, CSIRO Marine and Atmospheric Research, 2001.

Prata, A. J.: Satellite detection of hazardous volcanic clouds and the risk to global air traffic, Nat. Hazards, 51 (2), 303–324, 2009.

Pugnaghi, S., Guerrieri, L., Corradini, S., Merucci, L., and Arvani, B.: A new simplified approach for simultaneous retrieval of SO2 and ash content of tropospheric volcanic clouds: an application to the Mt Etna volcano, Atmos. Meas. Tech., 6, 1315-1327, doi:10.5194/amt-6-1315-2013, 2013.

Rose, W. I., Delene, D. J., Schnelder, D. J., Bluth, G. J. S., Krueger, A. J., Sprod, I., McKee, C., Davies, H. L., and Ernst, G. G. J.: Ice in the 1994 Rabaul eruption cloud - Implications for volcano hazard and atmospheric effects, Nature, 375 (6531), 477–479, 1995.

Rose, W. I., Bluth, G. J. S., and Watson, I. M.: Ice in volcanic clouds: When and Where?, Proceedings of the 2nd International Conference on Volcanic Ash and Aviation Safety, OFCM Washington D. C., Session 3, 61, 2004.

Scollo S., Boselli A., Coltelli M., Leto, G., Pisani, G., Spinelli, N., and Wang, X.: Monitoring Etna volcanic plumes using a scanning LiDAR, Bull. Volcanol., DOI 10.1007/s00445-012-0669-y, 2012.

Scollo, S., Prestifilippo, M., Pecora, E., Corradini, S., Merucci, L., Spata, G., and Coltelli, M.: Eruption Column Height Estimation: the 2011-2013 Etna lava fountains, Annals Of Geophysics, 57, 2, S0214; doi:10.4401/ag-6396, 2014.

Volz, F. E.: Infrared optical constants of ammonium sulfate, Sahara dust, volcanic pumice and fly ash, Appl. Opt., 12, 564–568, 1973.

Wen, S., and Rose, W. I.: Retrieval of sizes and total masses of particles in volcanic clouds using AVHRR bands 4 and 5, J. Geophys. Res., 99, 5421–5431, 1994.

Atmos. Meas. Tech. Discuss., doi:10.5194/amt-2015-390, 2016
Manuscript under review for journal Atmos. Meas. Tech.
Published: 17 February 2016

Atmospheric Measurement Techniques
Discussions

Table 1: Parameter values of the parabolic fit shown in Fig. 3a.

$(-\alpha)$	$\left(L_o + \alpha - B_p \cdot \tau^{''} - L_{uo}^{''}\right)$	$\left(B_p \cdot \tau^{''} + L_{uo}^{''}\right)$
a_2	a_1	a_0
-1.58	6.92	3.23

Atmos. Meas. Tech. Discuss., doi:10.5194/amt-2015-390, 2016
Manuscript under review for journal Atmos. Meas. Tech.
Published: 17 February 2016

Atmospheric Measurement Techniques Discussions
Open Access

Table 2: Polynomial coefficients to compute $\tau_{a,8.7}$ from $\tau_{a,11}$ for the pumice (Volz, 1973) ash type.

Satellite	$\boldsymbol{a_{3,8.7}}$	$\boldsymbol{a_{2,8.7}}$	$\boldsymbol{a_{1,8.7}}$	$\boldsymbol{a_{0,8.7}}$
Terra	0.1645	-0.4249	1.2559	0.0050
Aqua	0.1412	-0.3483	1.2028	0.0046

Table 3: Main characteristics of synthetic image, indicated as "True", together with the results of the VPR procedure, both new and old versions. The air temperature at 7.5 km was used as input for the VPR. The percentage differences are shown in brackets.

Mt. Etna – Pumice; 23 October 2013 plume altitude 7-8 km	**True**	**VPR new**	**VPR old**
Mean R_e (µm) (% difference)	2.85	2.92 (2.5)	4.80 (68.4)
Mean δ^* (% difference)	0.25	0.22 (-12)	0.19 (-24)
$R_e < 2\ \mu m$ Fine particles (%)	42	42	21
$2\ \mu m < R_e < 5\ \mu m$ Mean particles (%)	42	46	42
$R_e > 5\ \mu m$ Coarse particles (%)	16	12	37
Ash mass (t) (% difference)	8336	7812 (-6.3)	7166 (-14.0)
Pixels detected with ash	7533	7533	7317
SO_2 mass (t) (% difference)	19636	17146 (-12.7)	18880 (-3.9)
Pixels detected with SO_2	7533	7533	7533

Atmos. Meas. Tech. Discuss., doi:10.5194/amt-2015-390, 2016
Manuscript under review for journal Atmos. Meas. Tech.
Published: 17 February 2016

Table 4: Main characteristics of synthetic image, indicated as "True", together with the results of the VPR procedure, both new and old versions. The air temperature at 4.5 km was used as input for the VPR. The percentage differences are shown in brackets.

Eyjafjallajökull - Andesite **11 May 2010 14:05; plume altitude 4-5 km**	**True**	**VPR new**	**VPR old**
Mean R_e (μm) (% difference)	2.83	2.62 (-7.4)	3.3 (16.6)
Mean δ^* (% difference)	0.28	0.29 (+3.6)	0.39 (39.3)
$R_e < 2\ \mu m$ Fine particles (%)	43	46	38
$2\ \mu m < R_e < 5\ \mu m$ Mean particles (%)	42	44	46
$R_e > 5\ \mu m$ Coarse particles (%)	15	10	16
Ash mass (t) (% difference)	13227	12006 (-9.2)	9674 (-26.9)
Pixels detected with ash	10624	10624	6532
SO_2 mass (t) (% difference)	30724	28714 (-6.5)	28235 (-8.1)
Pixels detected with SO_2	10624	10624	9827

Atmos. Meas. Tech. Discuss., doi:10.5194/amt-2015-390, 2016
Manuscript under review for journal Atmos. Meas. Tech.
Published: 17 February 2016

Atmospheric Measurement Techniques Discussions

1

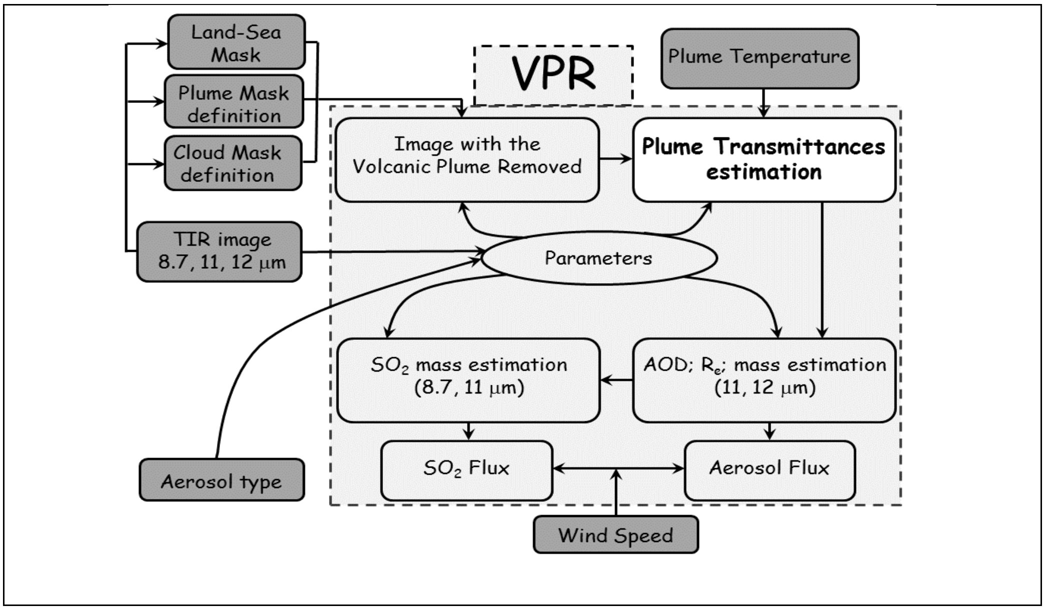

2 Figure 1. Flowchart illustrating the main steps of the VPR procedure.

3

Atmos. Meas. Tech. Discuss., doi:10.5194/amt-2015-390, 2016
Manuscript under review for journal Atmos. Meas. Tech.
Published: 17 February 2016

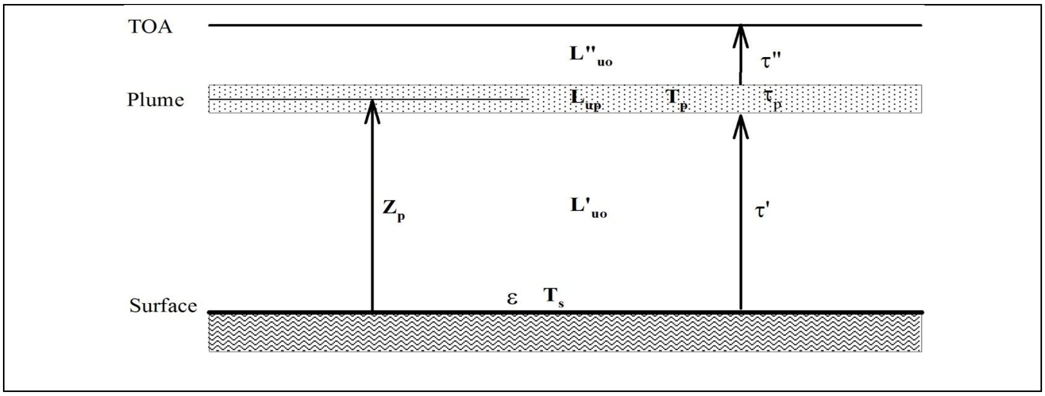

1 Figure 2. Scheme of the atmospheric model used in the improved VPR.

Atmos. Meas. Tech. Discuss., doi:10.5194/amt-2015-390, 2016
Manuscript under review for journal Atmos. Meas. Tech.
Published: 17 February 2016

Atmospheric Measurement Techniques
Open Access
Discussions

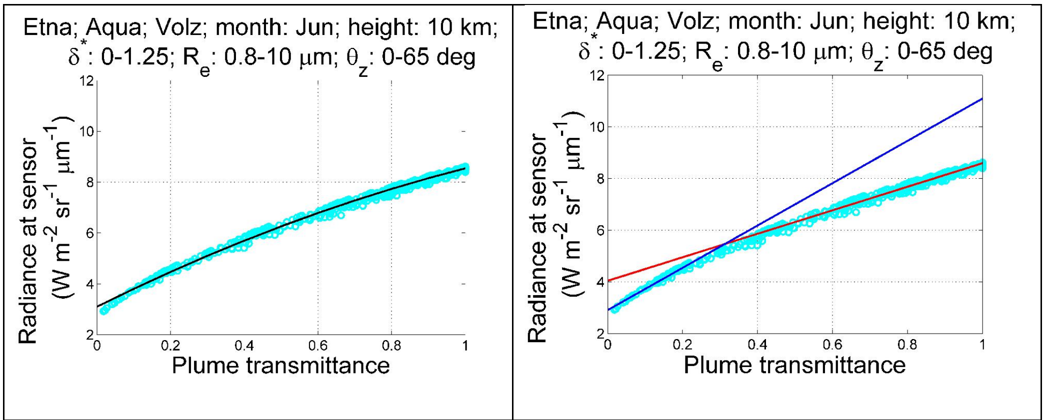

a)	b)

Figure 3. a) Radiances at the sensor (11 μm) vs. plume transmittances and their parabolic fit (black line); b) Same radiances with the two linear fits of Eq. (2) for the more transparent part of the plume (upper fit, red line), and Eq. (3) for the most opaque part of the plume (lower fit, blue line).

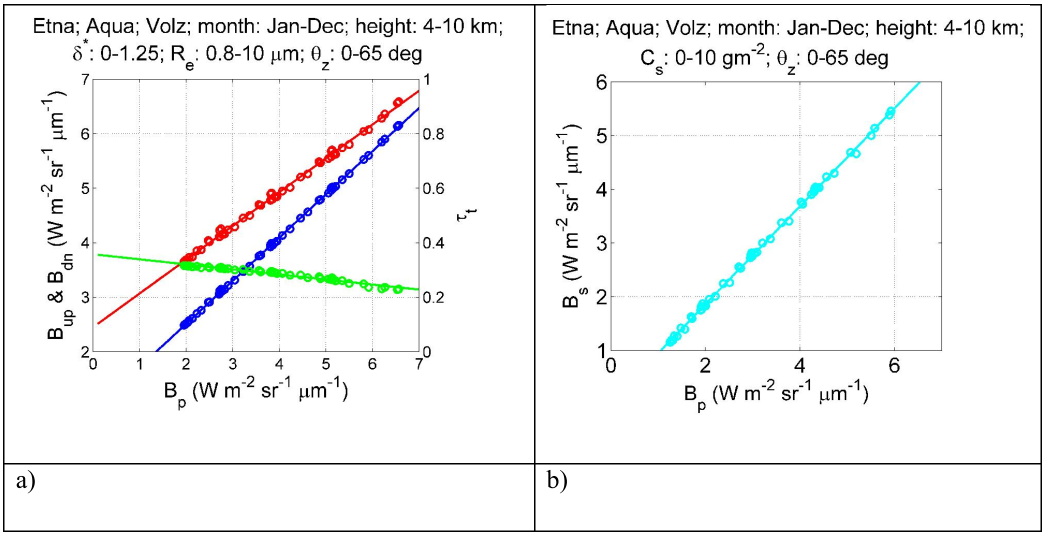

1 Figure 4. Linear trends of B_{up} (red), B_{dn} (blue), τ_t (green), and B_s (cyan) versus $\boldsymbol{B_p}$ for 48 different plumes (12 months and 4 heights) each obtained from a set of MODTRAN simulations.

Atmos. Meas. Tech. Discuss., doi:10.5194/amt-2015-390, 2016
Manuscript under review for journal Atmos. Meas. Tech.
Published: 17 February 2016

Atmospheric Measurement Techniques
Discussions

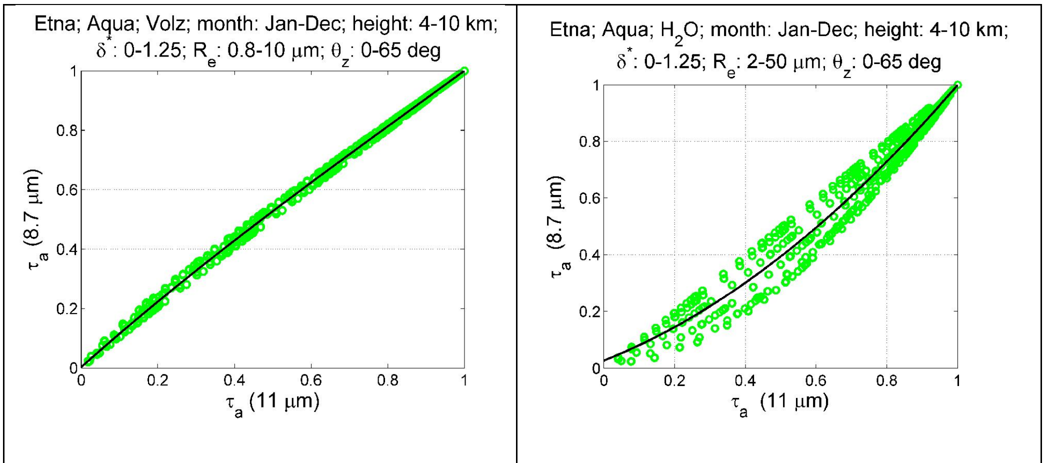

a)	b)

Figure 5. Scatter plots between the plume transmittance (obtained from a wide set of MODTRAN simulations) for MODIS-Aqua bands at 11 and 8.7 μm for the pumice (Volz, 1973) ash type (a), and for water droplets (b).

Atmos. Meas. Tech. Discuss., doi:10.5194/amt-2015-390, 2016
Manuscript under review for journal Atmos. Meas. Tech.
Published: 17 February 2016

Atmospheric Measurement Techniques Discussions

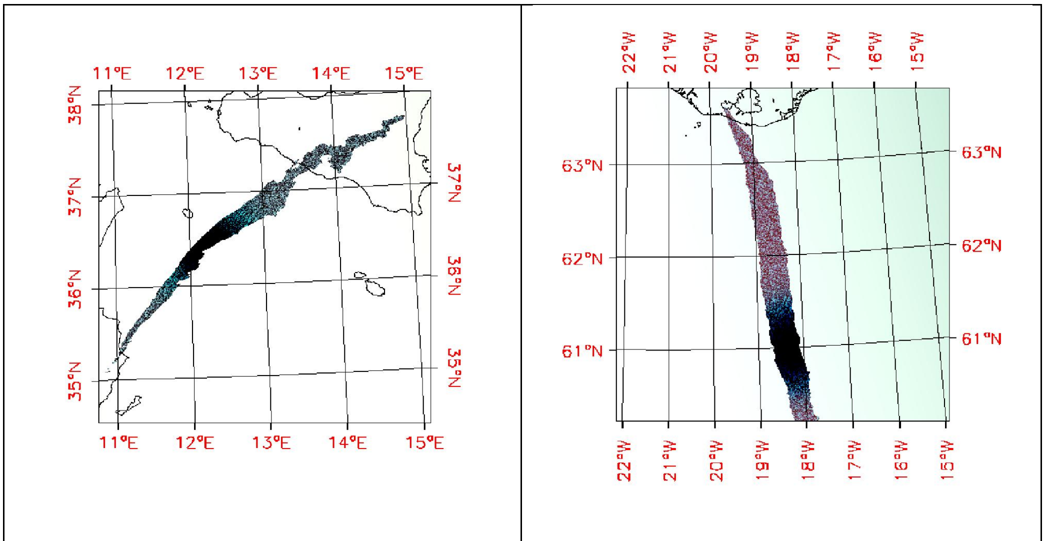

a) b)

1 Figure 6. Synthetic images (radiance at the sensor); RGB: bands at 8.7, 11, and 12 μm respectively.
2 a) Mt. Etna 26 October 2013 at 12:20 GMT; b) Eyjafjallajökull 11 May 2010 at 14:05 GMT
3

Atmos. Meas. Tech. Discuss., doi:10.5194/amt-2015-390, 2016
Manuscript under review for journal Atmos. Meas. Tech.
Published: 17 February 2016

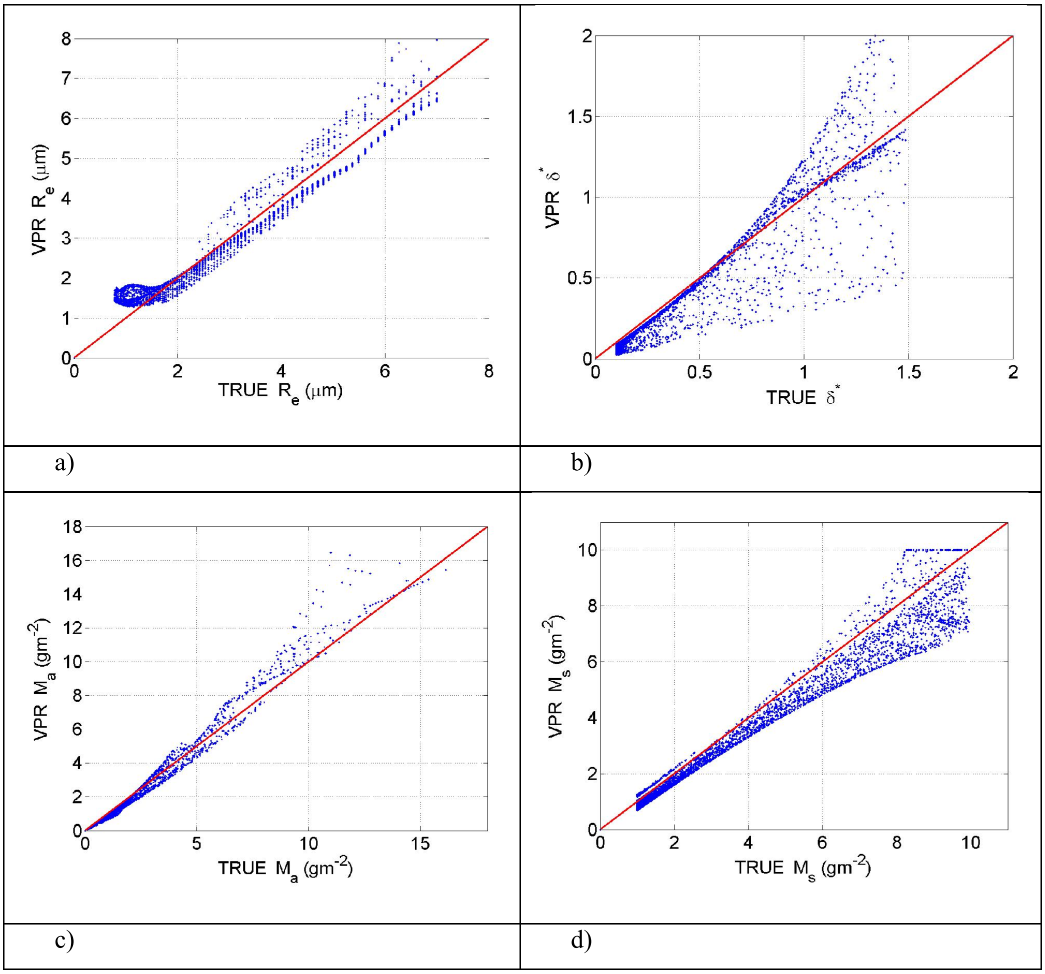

Figure 7. Etna-Pumice example: scatter plots between VPR results and true values: effective radius (a), ash optical depth at 550 nm (b), ash mass (c), and SO_2 mass (d). Red line is the bisector.

Atmos. Meas. Tech. Discuss., doi:10.5194/amt-2015-390, 2016
Manuscript under review for journal Atmos. Meas. Tech.
Published: 17 February 2016

Atmospheric Measurement Techniques Discussions
Open Access

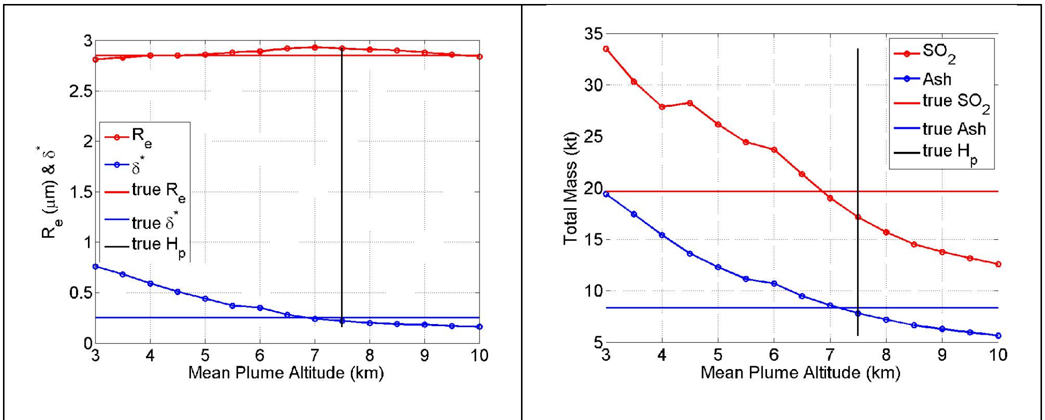

a) b)

Figure 8. Etna-Pumice example: trends of R_e and δ^* mean values (a), and ash and SO_2 total mass (b) retrieved by VPR with different input plume altitudes.

Atmos. Meas. Tech. Discuss., doi:10.5194/amt-2015-390, 2016
Manuscript under review for journal Atmos. Meas. Tech.
Published: 17 February 2016

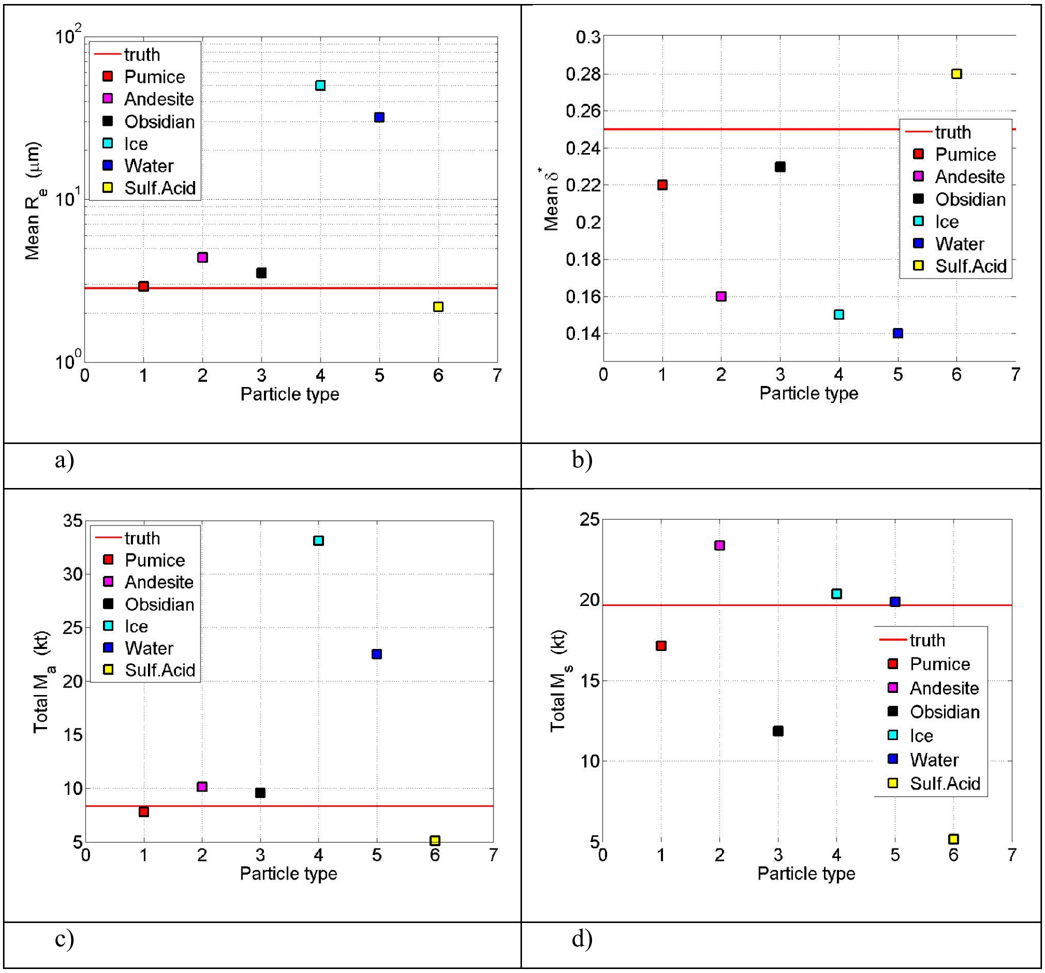

Figure 9. Etna-Pumice example. VPR results with different types of particles: mean effective radius (a), mean optical depth at 550 nm (b), total mass (c), and total SO_2 mass (d). The red lines are the true values.

Atmos. Meas. Tech. Discuss., doi:10.5194/amt-2015-390, 2016
Manuscript under review for journal Atmos. Meas. Tech.
Published: 17 February 2016

Atmospheric Measurement Techniques
Discussions

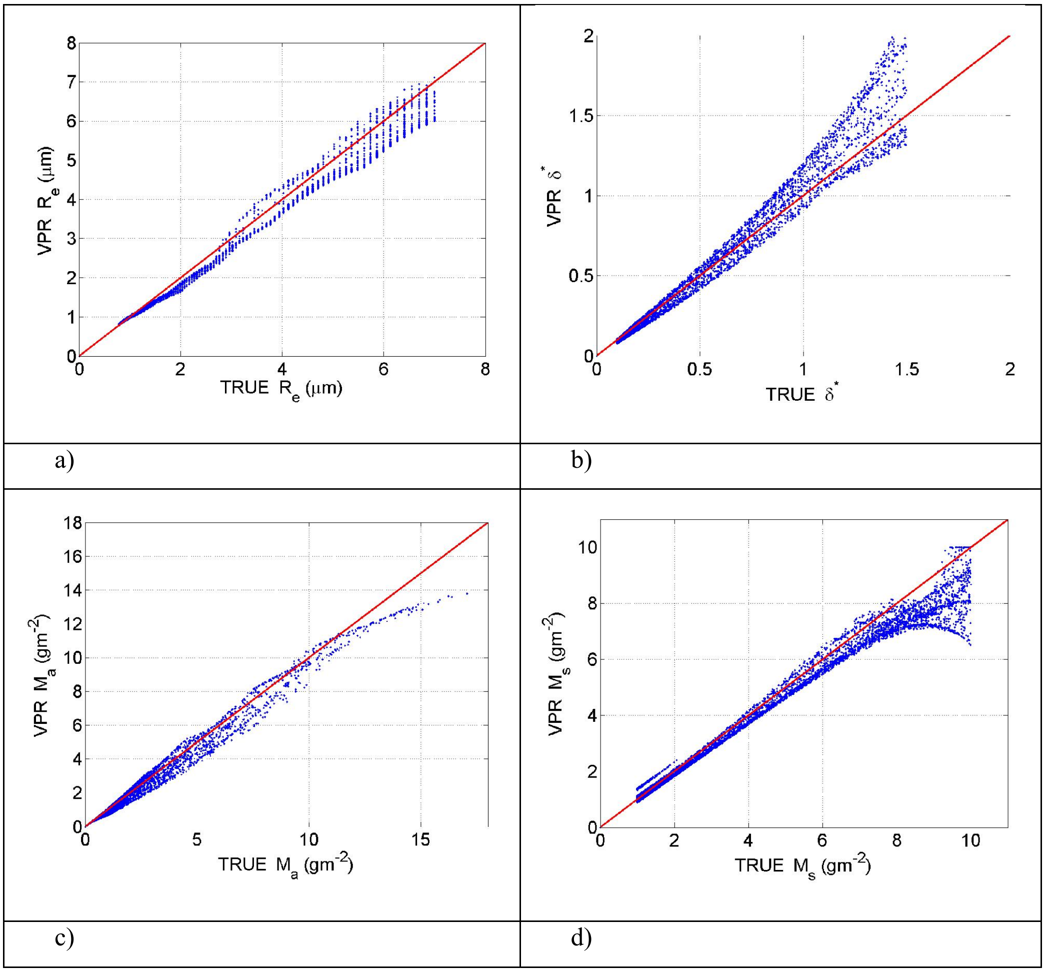

Figure 10. Eyjafjallajökull-Andesite example: scatter plots between VPR results and true values: effective radius (a), ash optical depth at 550 nm (b), ash mass (c), and SO_2 mass (d). Red line is the bisector.

Atmos. Meas. Tech. Discuss., doi:10.5194/amt-2015-390, 2016
Manuscript under review for journal Atmos. Meas. Tech.
Published: 17 February 2016

Atmospheric Measurement Techniques
Discussions
Open Access

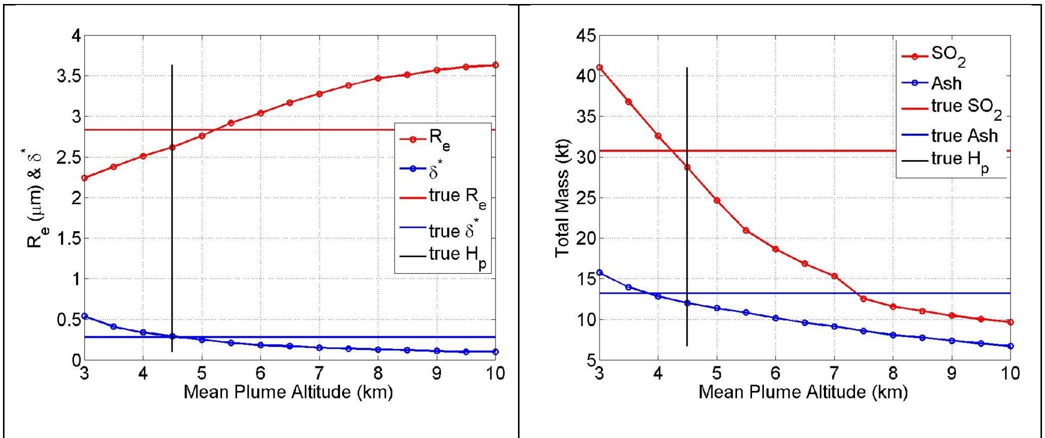

a) b)

1 Figure 11. Eyjafjallajökull-Andesite example: trends of R_e and δ^* mean values (a), and ash and SO_2
2 total mass (b) retrieved by VPR with different input plume altitudes.
3

Atmos. Meas. Tech. Discuss., doi:10.5194/amt-2015-390, 2016
Manuscript under review for journal Atmos. Meas. Tech.
Published: 17 February 2016

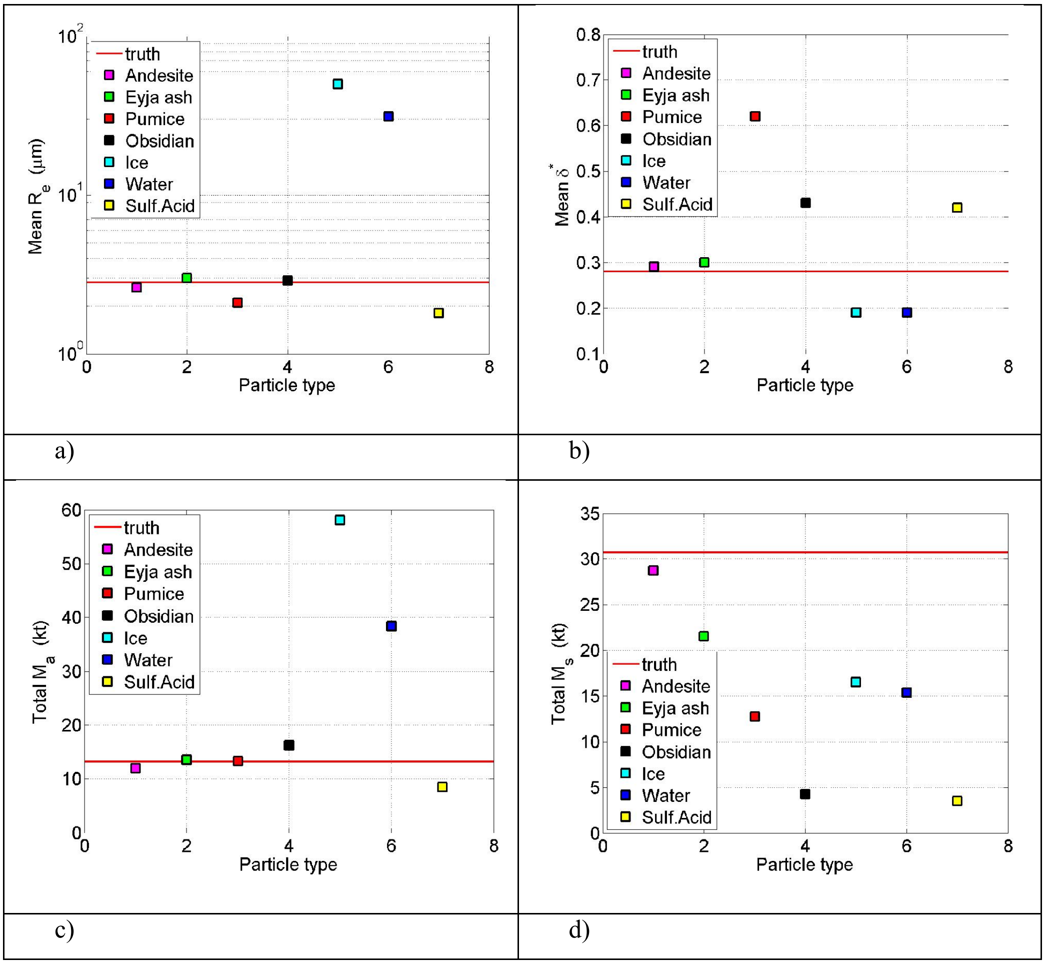

Figure 12. Eyjafjallajökull-Andesite example. VPR results with different types of particles: mean effective radius (a), mean optical depth at 550 nm (b), total mass (c), and total SO_2 mass (d). The red lines are the true values.